Title

Defining hydrogel properties to instruct lineage- and cell-specific mesenchymal differentiation

Authors

Hung, Ben P
Harvestine, Jenna N
Saiz, Augustine M
et al.

Publication Date

2019

DOI

10.1016/j.biomaterials.2018.10.024

Peer reviewed

Biomaterials 189 (2019) 1–10

Contents lists available at ScienceDirect

Biomaterials

journal homepage: www.elsevier.com/locate/biomaterials

Defining hydrogel properties to instruct lineage- and cell-specific mesenchymal differentiation

Ben P. Hung[a], Jenna N. Harvestine[a], Augustine M. Saiz[b], Tomas Gonzalez-Fernandez[a], David E. Sahar[c], Mark L. Weiss[d], J. Kent Leach[a,b,*]

[a] Department of Biomedical Engineering, University of California, Davis, Davis, CA 95616, USA
[b] Department of Orthopaedic Surgery, UC Davis Health, Sacramento, CA 95817, USA
[c] Department of Surgery, Division of Plastic Surgery, UC Davis Health, Sacramento, CA 95817, USA
[d] Department of Anatomy and Physiology, Kansas State University, Manhattan, KS 66506, USA

ARTICLE INFO

Keywords:
Spheroid
Design-of-Experiments
Alginate
Phenotype retention

ABSTRACT

The maintenance and direction of stem cell lineage after implantation remains challenging for clinical translation. Aggregation and encapsulation into instructive biomaterials after preconditioning can bolster retention of differentiated phenotypes. Since these procedures do not depend on cell type or lineage, we hypothesized we could use a common, tunable platform to engineer formulations that retain and enhance multiple lineages from different cell populations. To test this, we varied alginate stiffness and adhesive ligand content, then encapsulated spheroids of varying cellularity. We used Design-of-Experiments to determine the effect of these parameters and their interactions on phenotype retention. The combination of parameters leading to maximal differentiation varied with lineage and cell type, inducing a 2–4-fold increase over non-optimized levels. Phenotype was also retained for 4 weeks in a murine subcutaneous model. This widely applicable approach can facilitate translation of cell-based therapies by instructing phenotype *in situ* without prolonged induction or costly growth factors.

1. Introduction

Cell-based tissue engineering is a promising strategy to address the excessive demand for transplant tissue, which greatly outstrips supply. The examination of multipotent stem and progenitor cells has been pursued for nearly three decades due to the difficulty in procuring primary tissue-specific cells. Notably, the marrow-derived mesenchymal stem/stromal cell (MSC) is the most widely studied of these populations. Originally characterized with the ability to differentiate to adipogenic, chondrogenic, and osteogenic lineages [1], recent studies have reported their trophic factor secretion [2] as an important mechanism for promoting regeneration. Since the initial characterization of MSCs, studies on cell populations with similar potencies and self-renewal capabilities, such as the adipose-derived stem/stromal cell (ASC) [3] and the umbilical cord derived stem/stromal cell (UCSC) [4,5], have shown promise as alternative sources for cell-based therapies. Recent reports have focused on the biochemical and biological differences, such as in epigenetic modification [6,7] or in differentiation [8,9], which merit special consideration when applied for tissue regeneration or engineering.

MSCs, ASCs, and UCSCs can be reproducibly induced toward a fat, cartilage, or bone phenotype *in vitro* when stimulated by potent soluble cocktails of lineage-specification factors. Once implanted *in vivo*, however, these chemical cues are removed and continued control of cell fate remains challenging. Direct transplantation of cells into harsh, often inflammatory or hypoxic wound environments results in widespread and rapid cell death [10,11]. The delivery of cells with growth or lineage-specification factors, while promising for regenerating tissue prior to cell death, faces difficulties in clinical translation owing to the high costs and safety concerns [12]. Extended *in vitro* maturation of tissue grafts for transplantation, often investigated in the context of sophisticated bioreactor design, faces similar issues [13,14].

To address these challenges, we and others have investigated stem cell self-assembly into spheroids, which enhances viability and trophic factor secretion. Previously, we harnessed the potential of spheroid culture to retain the differentiated phenotype of MSCs that were preconditioned toward the osteogenic lineage [15], hypothesizing that the retention of endogenous extracellular matrix (ECM) would continue instructing the cells in the absence of exogenous signals. Interestingly, the entrapment of spheroids in alginate functionalized with the cell

* Corresponding author. 451 Health Science Dr, 2303 GBSF Davis, CA 95616, USA.
E-mail address: jkleach@ucdavis.edu (J.K. Leach).

https://doi.org/10.1016/j.biomaterials.2018.10.024
Received 28 August 2018; Received in revised form 15 October 2018; Accepted 19 October 2018
Available online 22 October 2018

binding motif Arg-Gly-Asp (RGD) also enhanced bone formation post-implantation [16], suggesting a complex interplay between cell-cell, cell-matrix, and cell-biomaterial interactions that influence cell fate. Taken together, these observations lead to the hypothesis that an engineered combination of aggregation and instructive biomaterial properties could retain and enhance lineage specification, even if specification only occurred within a brief preconditioning phase. This material-based approach is broadly applicable, as the same material building blocks and procedures could enhance several lineages from multiple cell types. To this end, we selected alginate for its tunable biomechanical and biochemical properties [17]. We varied the stiffness of alginate through its molar mass and the level of cellular interaction through the amount of RGD conjugated to each chain. We then demonstrated the wide applicability of this singular platform to retain and enhance the mesenchymal differentiation – adipogenesis, chondrogenesis, and osteogenesis – of MSCs, ASCs, and UCSCs.

2. Materials and methods

2.1. Isolation and culture of cells

Cryopreserved human MSCs were obtained from Lonza (Walkersville, MD) and RoosterBio (Frederick, MD) and used at passage 3, while ASCs [18] were obtained at the UC Davis Medical Center following Institutional Review Board (IRB)-approved protocols and with patient consent. Lipoaspirate was digested in collagenase (Worthington, Lakewood, NJ) and centrifuged to remove adipocytes, followed by washes to remove other cell types and tissue fragments. The pellet was termed the stromal vascular fraction (SVF) and plated (at which point they were termed ASCs) for the outlined experiments. Human UCSCs were isolated at Kansas State University per previously published protocols and under an approved IRB with patient consent [19]. Umbilical cords were cut into 1-cm sections and dissociated both enzymatically and mechanically using collagenase I + hyaluronidase (Thermo Fisher Scientific) and a gentleMACS™ dissociator (Miltenyi Biotec, Bergisch Gladbach, Germany), respectively. Erythrocytes were removed prior to plating isolated UCSCs. UCSCs were used at passage 6 for this study.

All populations were expanded until confluency prior to lineage-specific induction. For MSCs and ASCs, expansion medium consisted of Dulbecco's Modified Eagle Medium (DMEM) with 4.5 g/L glucose (Thermo Fisher Scientific, Waltham, MA) supplemented with 100 U/mL penicillin and 100 μg/mL streptomycin (Cellgro, Manassas, VA), 10% v/v fetal bovine serum (FBS, Atlanta Biologicals, Flowery Branch, GA), and 2 mM L-glutamine (Thermo Fisher Scientific). UCSC expansion medium was the same except FBS was replaced with 10% v/v Stemulate human platelet lysate (hPL, Cook Regentec, Indianapolis, IN) per previous protocols [19]. Lineage-specific medium formulations were held constant for all cell types as outlined in Table 1 [8,20–22]. All reagents used in the medium formulations were from Sigma-Aldrich except for transforming growth factor β3, which was sourced from PeproTech (Rocky Hill, NJ).

Table 1
Lineage-specific medium formulations.

Adipogenic	Chondrogenic	Osteogenic
• MSC/ASC expansion medium • 5 μg/mL recombinant human insulin • 1 μM dexamethasone • 200 μM indomethacin • 500 μM 3-isobutyl-1-methylxanthine	• MSC/ASC expansion medium without FBS • 1 μM dexamethasone • 10 ng/mL transforming growth factor β3 • 50 μM ascorbic acid • 40 μg/mL L-proline • 110 μg/mL sodium pyruvate • ITS: 10 μg/mL bovine insulin, 5.5 μg/mL human transferrin, 6.7 ng/mL selenium	• MSC/ASC expansion medium • 10 mM β-glycerophosphate • 50 μg/mL ascorbic acid

2.2. Experimental workflow

Cells were plated at 5,000 cells/cm^2 in monolayer and allowed to reach confluency before lineage specific medium was applied (Fig. 1a). One group was maintained in expansion conditions as a negative control. This preconditioning phase was carried out for 1 week prior to detachment *via* trypsin-EDTA (Corning, Corning, NY) and aggregation (Fig. 1b) into spheroids of 3,000 to 10,000 cells per spheroid. Spheroids were then collected and encapsulated in alginate gels for culture in expansion conditions for an additional two weeks (Fig. 1c). This expansion culture was meant to simulate post-implantation conditions where no exogenous lineage-specific factors would be present. Expansion medium in this phase was supplemented with 2 mM β-glycerophosphate to ensure the osteogenic lineage had a phosphate source to mineralize while not providing the full concentration, which could act as an osteogenic signal while potentially resulting in dystrophic mineralization [23]. Alginate stiffness was varied by manipulating the molar mass, which ranged from 100% of 21 mg/mL 1 kg/mol alginate (LM alginate) to 100% of 21 mg/mL 50 kg/mol (HM alginate). The mechanical properties of the alginate were determined by rheology (TA Instruments, New Castle, DE) using a strain sweep from 0.004 to 0.04 at 10 rad/s [16]. Alginate groups also had variable RGD content, ranging from no RGD to 8 RGD ligands per alginate chain.

2.3. Spheroid formation

Aggregation of preconditioned cells followed previous protocols [24,25]. Briefly, monodisperse cells were pipetted into an agarose mold of known dimensions and centrifuged to pellet the cells within the microwells. The number of cells per spheroid was controlled by the initial concentration in the cell suspension. Cells were allowed to self-aggregate into spheroids over two days in expansion medium.

2.4. RGD conjugation to alginate

Covalent conjugation of RGD (G_4-RGD-SP, Commonwealth Biotechnologies, Richmond, VA) to the alginate (Pronova, Sandvika, Norway) followed previously established protocols using carbodiimide chemistry [16]. The molar ratio of RGD to alginate was varied such that each alginate chain possessed a degree of substitution (DS) of 0, 4, or 8. The DS is a measure of how many motifs on average are present on each alginate chain. The alginate was then lyophilized for one week and resuspended in phosphate-buffered saline at 21 mg/mL for encapsulation of cells. We employed a modified ninhydrin assay to confirm the success of the conjugation. Because ninhydrin does not react with amides, we used 0.5 M sodium hydroxide to break the amide bonds and form primary amines, which could then be detected using ninhydrin reagent as reported previously [26].

2.5. Alginate gelation and spheroid encapsulation

Spheroids were encapsulated in alginate and pipetted into an 8-mm diameter, 1.5-mm height silicone mold. A 6–8 kDa molar mass cutoff dialysis membrane (Spectrum Labs, Rancho Dominguez, CA) was overlaid on the alginate and a 200 mM solution of $CaCl_2$ was allowed to dialyze against the alginate for 10 min, followed by 5 min of incubation in $CaCl_2$ in direct contact with the alginate gel [16].

2.6. Trilineage assessments

Adipogenesis was assessed *via* Oil Red O staining for lipid droplets both qualitatively [20,22] and quantitatively; for the latter, 100% isopropanol was used to elute the stain and the absorbance was read at

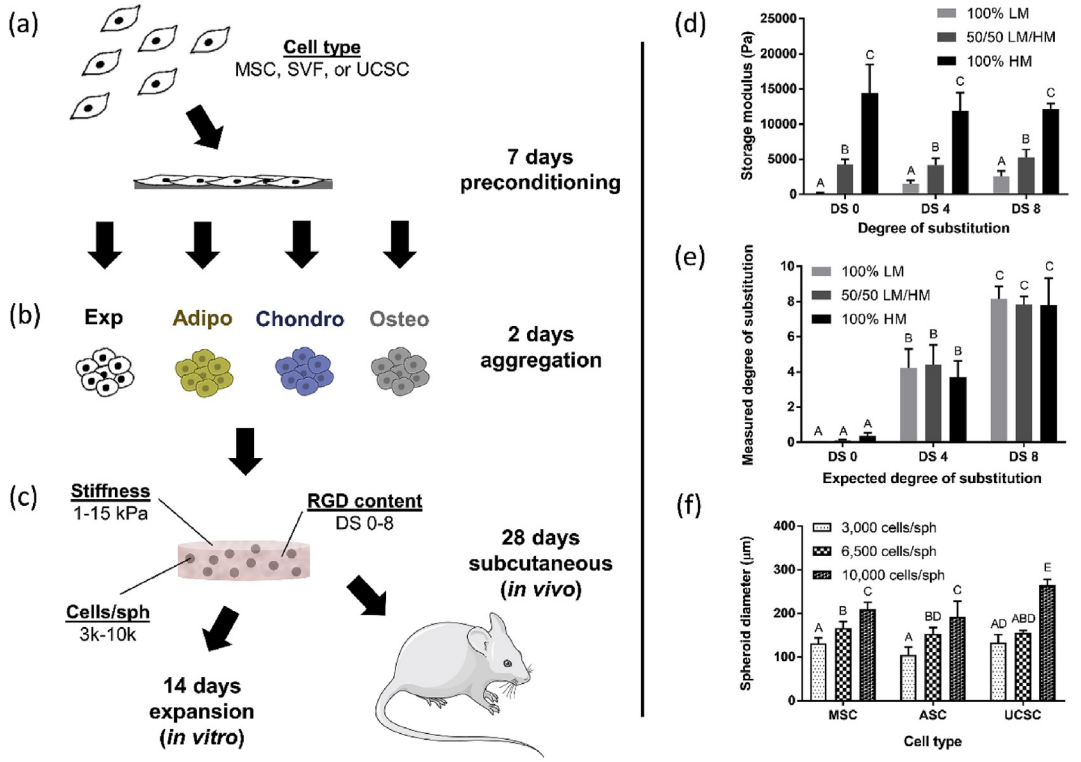

Fig. 1. Experimental workflow and component characterization. (**a**) MSCs, SVF, or UCSCs were plated, expanded to confluence, and preconditioned for 7 days under adipogenic, chondrogenic, or osteogenic conditions. A control group consisted of continued expansion culture for the 7-day period. (**b**) Preconditioned cells were aggregated into spheroids of 3,000, 6,500, or 10,000 cells and encapsulated into alginate hydrogels of 1 kg/mol (LM), 50 kg/mol (HM), or a 50/50 mixture of the two and 0, 4, or 8 RGD motifs per alginate chain (DS). (**c**) Constructs were cultured under expansion conditions for 2 weeks for *in vitro* assessments or 4 weeks in the murine subcutaneous model. (**d**) Rheological measurements of alginate showed a range of 1–15 kPa storage modulus corresponding to 1–50 kg/mol. (**e**) Ninhydrin assessments confirmed the presence of RGD in the expected amounts. (**f**) Spheroid diameter increased with increasing cells per spheroid. Each bar represents $n = 3$. Bars with different letters are statistically different based on a two-way ANOVA with $p < 0.05$. Data are mean ± standard deviation.

510 nm [27,28]. Chondrogenesis was assessed qualitatively *via* Safranin O staining for glycosaminoglycan (GAG) content [20] and quantitatively using 1,9-dimethylmethylene blue (Sigma Aldrich) with special attention to pH, set to 1.5, to prevent false negative signal from the alginate itself [29]. Osteogenesis was assessed qualitatively *via* Alizarin Red S staining for protein-associated calcification [8,21] and quantitatively using *o*-cresolphthalein complexation [8,20,21,28] for calcium content. In all quantitative assessments, markers were normalized by using the Quant-iT PicoGreen dsDNA assay kit (Thermo Fisher Scientific) to quantify DNA and converting to cell number using a DNA-cell curve (*data not shown*).

2.7. Design-of-Experiments response surface analysis

Due to the large number of factors present in this investigation, we employed a Design-of-Experiments (DOE) approach to ensure the interactions between the factors were retained in the analysis. A Box-Behnken scheme was established in Design-Expert (Stat-Ease, Minneapolis, MN) in which the parameters under consideration were varied among three levels: low, middle, or high (Table 2). The quantitative outputs for the three lineages after the two-week expansion culture were then fit to a response surface model:

Table 2
Box-Behnken design.

Parameter	Low (−1)	Middle (0)	High (+1)
Alginate stiffness	100% LM	50/50 LM/HM	100% HM
RGD density	DS 0	DS 4	DS 8
Cells per spheroid	3,000	6,500	10,000

$$y = \beta_0 + \beta_s x_s + \beta_r x_r + \beta_c x_c + \beta_{ss} x_s^2 + \beta_{rr} x_r^2 + \beta_{cc} x_c^2 + \beta_{sr} x_s x_r + \beta_{rc} x_r x_c + \beta_{cs} x_c x_s \quad (1)$$

where y is the output (Oil Red O/cell, GAG/cell, or calcium/cell); the subscripts represent stiffness (s), RGD content (r), and cells per spheroid (c); β represents fitted coefficients; and x represents the coded variables: −1 for low, 0 for middle, and 1 for high. With Eqn. (1), we could determine the relative impact of each parameter along with their interactions. In addition, we used Eqn. (1) to determine input combinations leading to maximum and minimum outputs. These combinations were verified in two additional donors per cell type to test the accuracy of the model. In the rest of the report, these groups are denoted by the preconditioned lineage followed by (+) for maximal or (−) for minimal.

2.8. Mechanistic studies on migration

After preconditioning, aggregation, and encapsulation, UCSC spheroids were subjected to 2 μg/mL mitomycin C (Sigma-Aldrich) or no treatment for 4 days. DNA and protein content were measured each day with the Quant-iT PicoGreen dsDNA assay kit and the Pierce BCA Protein assay kit (Thermo Fisher Scientific) to verify that ECM protein per cell was higher in the treated group due to inhibited proliferation. Constructs were cultured under standard expansion medium for 3 days after the treatment period and imaged by brightfield microscopy to assess extent of migration from the spheroid.

2.9. Subcutaneous murine implantation

Treatment of experimental animals was in accordance with the UC Davis animal care guidelines and all National Institutes of Health

animal handling procedures. 8-week-old Nod-SCID-gamma (NSG) mice, 4 female and 4 male (UC Davis Institute of Regenerative Cures) were anesthetized by 2% isoflurane/oxygen mixture. The surgical site was shaved and cleaned with medical-grade alcohol and iodine. Each animal received 4 subcutaneous pockets dorsally, each pocket implanted with one construct containing 20×10^6 UCSCs/mL. The left superior pocket contained an adipogenic construct, the right superior pocket a chondrogenic construct, and the left inferior pocket an osteogenic construct. 2 of the females and 2 of the males received constructs representing the maximal differentiation predicted by the DOE, whereas the other mice received the constructs representing the minimal differentiation predicted by the DOE, ensuring that both genders were represented equally. The fourth pocket contained a construct with cells cultured only under expansion conditions as a negative control. Mice recovered without incident and were sacrificed 4 weeks post-implantation and constructs were excised for histological analysis.

2.10. Micro-computed-tomography (micro-CT) and histological analysis

After the constructs were recovered, they were fixed by immersion in 4% formalin overnight and scanned using micro-CT (Scanco Medical, Brüttisellen, Switzerland) with a 70 kVp X-ray source at 114 μA. Quantification was performed by setting a threshold of 200, corresponding to a density of 411.98 mg hydroxyapatite/cm^3 and the mineral volume (mm^3) was recorded [30]. Reconstructed 3D images were generated from the scans and used to visualize mineral distribution throughout the constructs.

Constructs were then dehydrated in a graded series of ethanol baths, embedded in paraffin wax, sectioned at 7 μm, and affixed to microscope slides as described [28,31]. Sections were stained with Harris hematoxylin and eosin (H&E) (Thermo Scientific) to assess bone and blood vessel formation and the presence of adipose tissue, Alcian Blue with aldehyde fuchsin (Sigma-Aldrich) to assess GAG content, and Picrosirius Red (Sigma Aldrich) to observe collagen production.

2.11. Statistical analysis

Statistical analysis in Fig. 1 was performed *via* a two-way ANOVA with significance at $p < 0.05$. In Fig. 5, a two-tailed *t*-test was performed within each timepoint (Fig. 5b) and within each lineage (Fig. 5c) with significance at $p < 0.05$.

3. Results

3.1. Characterization of biomaterial and spheroid parameters

Rheology measurements of 100% LM, 50/50 LM/HM, and 100% HM (Fig. 1d) confirmed the increase in storage modulus with increasing alginate molar mass, resulting in moduli ranging from 1 kPa (100% LM) to 15 kPa (100% HM). The desired quantity of RGD on the alginate backbone was observed using the ninhydrin assay (Fig. 1e). The modulus and the DS did not affect each other, allowing these parameters to be decoupled within the DOE scheme (Fig. 1d and e). Spheroid diameter was comparable between the cell types and increased with increasing cellularity (Fig. 1f). The diameters observed, between 100 and 200 μm, were comparable to those measured previously [32]. In agreement with previous studies, spheroid packing density – cell number per unit volume of spheroid – decreased with increasing cellularity, as evidenced by the diameters being higher than that predicted by geometrical models [32] (Fig. 5a).

3.2. Initial differentiation level and culture within alginate gels

We assessed the levels of Oil Red O, GAG, and calcium per cell both qualitatively and quantitatively immediately after the preconditioning phase (Fig. 2a). After only one week of induction, levels of differentiation markers were expectedly low, with GAG/cell at undetectable levels. The limited expression of chondrogenic ECM was unsurprising as cartilage formation is generally achieved in pellet culture with cell-cell contact [1,33] as opposed to the monolayer system used here. In addition, we observed differences in proliferation. While all cell types began the preconditioning phase at similar level of confluency, the UCSCs achieved the highest number of cells by the end of the preconditioning phase (Fig. 2a). While this could be due to the hPL in the UCSC expansion medium as opposed to FBS, the preconditioning phase consistently included FBS among all three cell types, suggesting an innately higher growth rate for UCSCs.

We observed morphological differences after 7 days in culture (Fig. 2b) when spheroids were entrapped in alginate. Specifically, unmodified alginate (no RGD) facilitated the maintenance of spherical aggregate morphology, while alginate with RGD allowed cells to attach and spread. Interestingly, the 100% LM alginate, despite containing RGD, did not support cell spreading morphology, suggesting that cells were able to pull the soft substrate toward the aggregate. Such phenomena are well-supported in previous studies where cell spreading was more pronounced on stiffer substrates [34].

3.3. Lineage specification is retained depending on the combination of input parameters

Following culture in maintenance conditions (*i.e.* no lineage-specific factors) for two weeks, we detected marked differences in the expression of differentiation markers (Fig. 3), suggesting that any combination of substrate modulus, RGD content, and cells per spheroid affected cell differentiation. Importantly, many of the levels were above the initial levels measured immediately after the preconditioning phase (Figs. 2a and 3). These data indicate that the phenotypes were retained, and the biomaterial/spheroid combination maintained the instruction toward the three lineages. ASCs performed the best in adipogenesis, achieving a ~6-fold change in Oil Red O absorbance per cell between initial and final levels. MSCs exhibited the greatest osteogenic potential, evidenced by a ~20-fold change in calcium/cell between initial and final levels. Instruction of phenotype was most apparent in the chondrogenic lineage, where no GAG was detectable immediately after preconditioning but increased up to 1.5 ng GAG/cell by the end of the expansion phase for all three cell types. Response surface analysis (Fig. 4a) revealed differences in the impact of key parameters as a function of both lineage and cell type. Nearly half of all fitted coefficients in Eqn. (1) had 95% confidence intervals not containing 0 (red bars, less than 0; green bars, greater than 0), indicating significant effects. In particular, about 20% of all interaction terms were significant, highlighting the importance of the DOE method when analyzing multifactorial systems. To elucidate how these parameters contributed to differentiation, we determined the locations of maxima and minima of Eqn. (1) in the 3D space where the axes are defined by 1–15 kPa stiffness, RGD DS 0–8, and 3,000–10,000 cells/spheroid (Fig. 4b). The location of maximal adipogenesis coincided with the location of minimal osteogenesis for all three cell types (dark gold and light grey points at 15 kPa, RGD DS 8, and 3,000 cells/spheroid), an observation in agreement with previous studies establishing the opposing nature of these two lineages [35]. The chondrogenic (+) location (dark blue points) was common between MSCs and ASCs at 1 kPa, RGD DS 8, and 3,000 cells/spheroid. In UCSCs, this point occurred at 15 kPa, RGD DS 0, and 3,000 cells/spheroid. Both of these formulations maintained aggregate morphology (Fig. 2b), which agrees with the conventional understanding of how cell-cell cohesion and aggregation promote chondrogenesis. The osteogenic (+) location (dark black points) varied the most between the three cell types. MSC osteogenic (+) occurred at 4.3 kPa, RGD DS 1.9, and 3,000 cells/spheroid; ASC osteogenic (+) occurred at 1 kPa, RGD DS 8, and 10,000 cells/spheroid; and UCSC osteogenic (+) occurred at 3.4 kPa, RGD DS 4, and 8,300 cells/spheroid. The formulations corresponding to all extrema were created

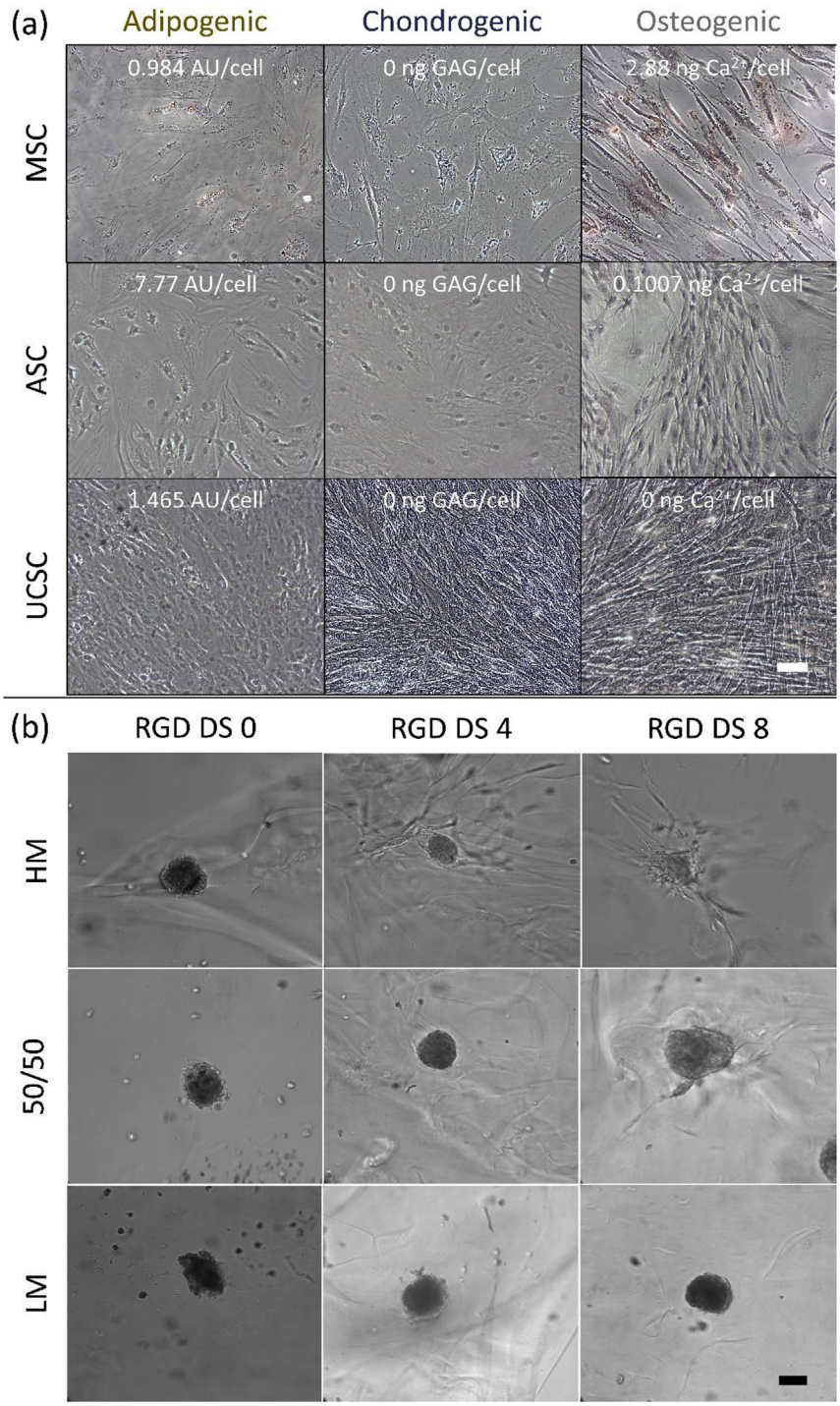

Fig. 2. Preconditioning and spheroid morphology. (**a**) Immediately after preconditioning, expression of differentiation markers was low for all three cell types as evidenced by Oil Red O (fat droplets), Safranin O (GAG), and Alizarin Red S (calcification) staining. Quantitative assessments *via* absorbance measurements of Oil Red O, DMMB assay for GAG, and OCPC assay for calcium per cell (numbers) confirmed these observations. (**b**) Spheroids showed varying morphology in the alginate groups after 1 week. High stiffness with high RGD content induced cell spreading and migration from the spheroid, while spherical morphology was preserved when no RGD was presented. Low stiffness gels also elicited the spherical morphology even with the presence of RGD. Scalebars: 200 μm (**a**), 100 μm (**b**). (For interpretation of the references to color in this figure legend, the reader is referred to the Web version of this article.)

and used to test 2 additional donors per cell type as verification of the model. While the magnitudes of the fold-change between the maxima and minima differed between donors, the trends remained consistent (Supplementary Fig. S1).

3.4. Enhanced migration results in higher adipogenesis and lower osteogenesis

We elected to focus on the adipogenic (+), osteogenic (−) combination – 15 kPa stiffness, RGD DS 8, and 3,000 cells per spheroid – due to its commonality among all three cell types and investigate its mechanistic effect. Based on the outputs (Fig. 3), UCSCs achieved the greatest fold change between initial and final levels, suggesting a higher degree of differentiation-induced plasticity. Thus, we utilized UCSCs for the remainder of the study.

We hypothesized that the extent of migration from the spheroid to the biomaterial may dictate cell phenotype. Spheroid osteogenesis is inversely related to MSC migration into RGD alginate [24]. On the other hand, extensive migration of preadipocytes into primitive fat organs characterizes early adipogenesis [36]. We further hypothesized that the relationship between intra-spheroidal ECM and cell number is a key parameter that dictates cell migration in engineered materials. Higher cell numbers per spheroid resulted in lower packing density (Fig. 5a and in agreement with our previous study [32]). More ECM is thus available for cell adhesion in larger spheroids compared to in smaller spheroids, allowing cells greater opportunity to access

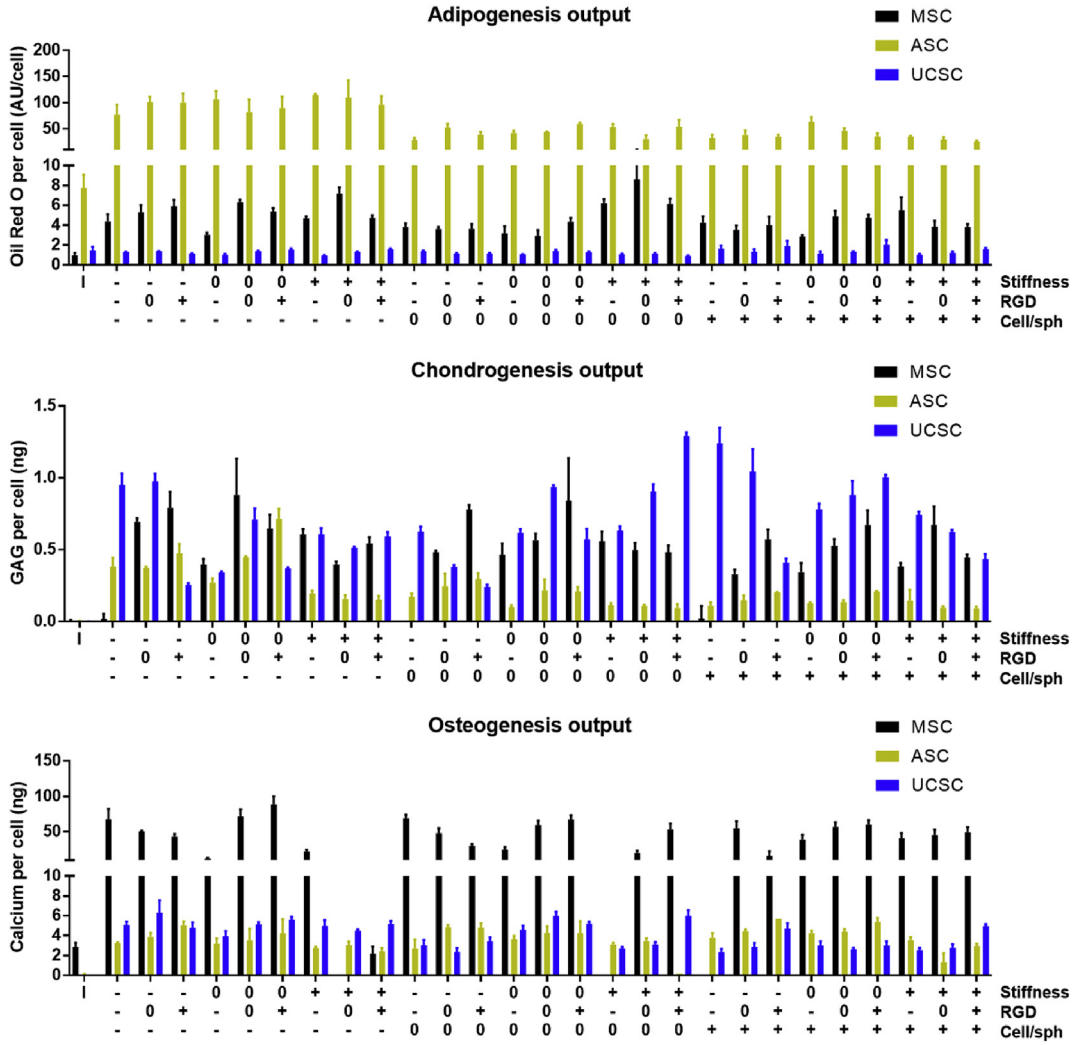

Fig. 3. Outputs for trilineage differentiation of all three cell types. To fit the DOE model, constructs representing all combinations of alginate stiffness, RGD content, and cells per spheroid for MSCs, ASCs, and UCSCs preconditioned under adipogenic, chondrogenic, and osteogenic conditions (27 groups per cell type per lineage) were cultured and assessed for Oil Red O absorbance per cell, GAG/cell, and calcium/cell. The leftmost bar labeled "I" indicates the level of initial outputs, *i.e.* measured immediately after the preconditioning phase. The biomaterial formulations, combined with spheroid aggregation, were able to retain and enhance phenotype as evidenced by the final output levels exceeding the initial. The variation in the outputs also suggests the different combinations of parameters affected the extent of phenotype retention and enhancement. (For interpretation of the references to color in this figure legend, the reader is referred to the Web version of this article.)

endogenous ECM *versus* the RGD on the alginate. We tested this hypothesis by applying mitomycin C to 10,000-cell spheroids, thereby inhibiting cell proliferation while leaving ECM production intact. Cell migration was markedly inhibited in mitomycin C-treated groups (Fig. 5b) and correlated with increased ECM available per cell.

Based on these findings, we speculated that the 3,000-cell spheroids would enable increased migration, as the relatively low number of cells per spheroid would result in higher packing density and therefore less ECM. We encapsulated adipogenically and osteogenically preconditioned UCSCs aggregated into 3,000-cell spheroids in either (1) DOE-predicted adipogenic (+)/osteogenic (−) alginate, or (2) the same formulation, but with the RGD not conjugated to the alginate. As expected, we observed little-to-no migration in the latter group compared to RGD-modified alginate (Fig. 5d). Reductions in migration correlated with reduced adipogenesis and increased osteogenesis compared to DOE predictions (Fig. 5c).

3.5. Phenotype retention persists in vivo

We excised constructs 4 weeks post-implantation from the murine subcutaneous tissue and scanned them using micro-CT. Mineral appeared in the adipogenic (−), osteogenic (+), and osteogenic (−) groups, with the maximal osteogenic group featuring the most mineral (Fig. 6). While the osteogenic (−) constructs contained mineral, the spatial distribution resembled a shell around the construct as opposed to distinct mineralized spheroids dispersed throughout in the other groups, suggesting that mineral deposition was due to more passive processes in the osteogenic (−) group as opposed to cell-mediated biomineralization. Picrosirius Red staining for collagen (Fig. 6) supports this interpretation, as collagen staining was localized to the spheroids in the adipogenic (−) and osteogenic (+) groups but not in the osteogenic (−) group.

We used Alcian Blue with aldehyde fuchsin counterstain for better visualization of GAG, as Alcian Blue by itself also stains alginate. Light purple staining for GAG was only apparent in the adipogenic (−) and chondrogenic (+) groups (Fig. 6). These data suggest the chondrogenic (+) group was successful in retaining chondrogenic phenotype, while the chondrogenic (−) group was not, as predicted by the DOE model. The presence of GAG staining in the adipogenic (−) group, along with the presence of mineralized spheroids in this group, is an interesting

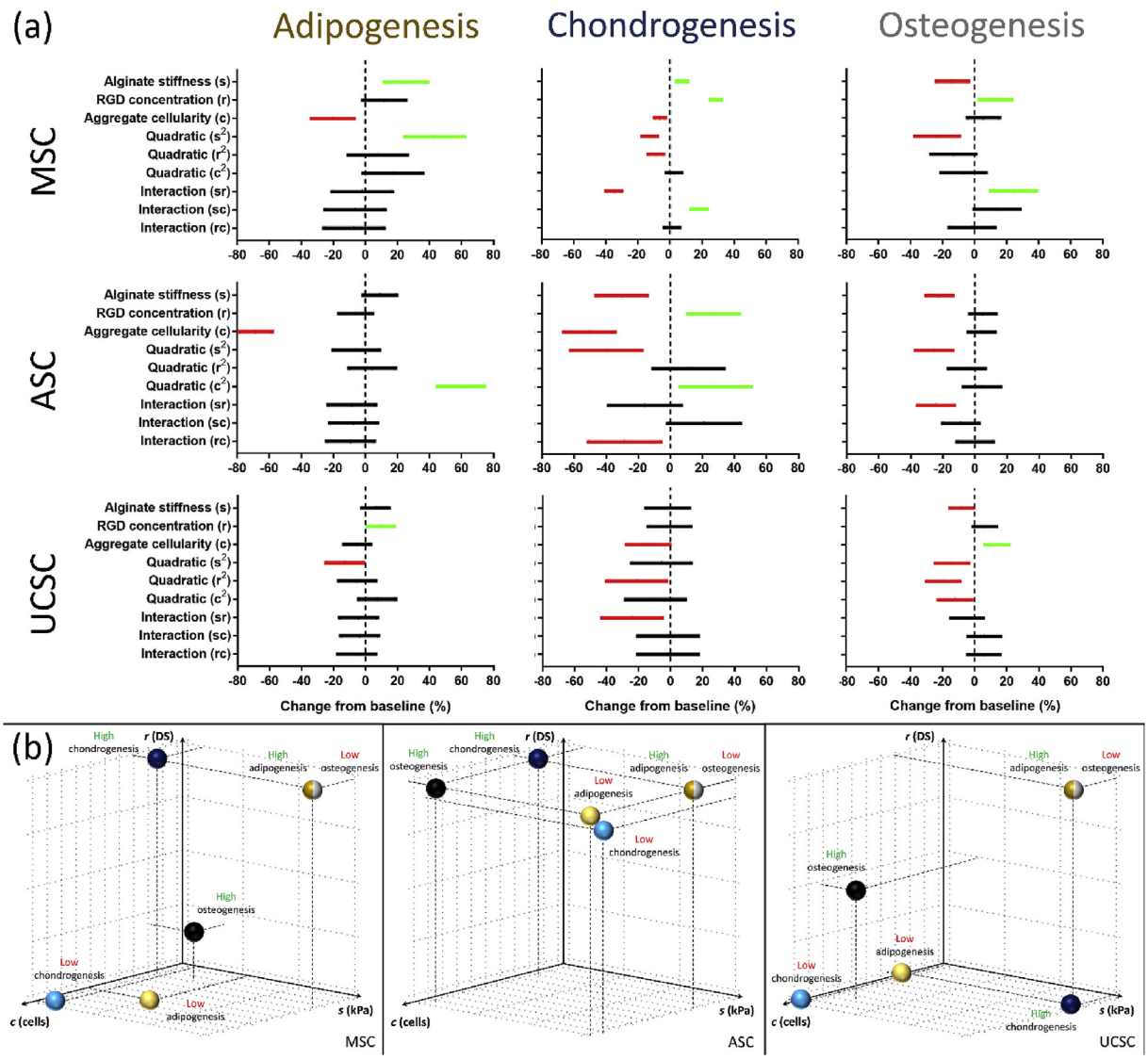

Fig. 4. DOE model predictions. (**a**) Coefficients in Eqn. (1) were determined by fitting Oil Red O absorbance, GAG/cell, and calcium/cell data as a function of stiffness, RGD content, and cells per spheroid. These coefficients represent the relative impact of each input and their interactions. Widths of bars indicate the 95% confidence interval of the fit where a green bar denotes a significant positive effect, a red bar denotes a significant negative effect, and a black bar indicates no statistical effect of the parameter on the output. (**b**) By using the fitted coefficients in Eqn. (1), the maximal and minimal locations of differentiation for the three lineages and three cell types were determined in the 3D space defined by the axes 1–15 kPa stiffness, RGD DS 0–8, and 3,000–10,000 cells/spheroid. In particular, the maximal adipogenic point coincided with the minimal osteogenic point, an observation that held for all three cell types. (●) = adipogenesis, (●) = chondrogenesis, and (●) = osteogenesis. Light colors indicate minimal levels while dark colors indicate maximal levels. (For interpretation of the references to color in this figure legend, the reader is referred to the Web version of this article.)

and unexpected result. Regardless, fat ghosts, artifacts of the effect of the histological processing on fat droplets, were only detected in the adipogenic (+) group, suggesting this group retained adipogenic phenotype while the adipogenic (−) constructs could not.

Spheroidal morphology also varied between the groups, with the adipogenic (−), chondrogenic (+), and osteogenic (+) groups featuring the most spheroidal structures. Incidentally, these groups possessed the lowest RGD conjugation, thereby discouraging cell migration and promoting the preservation of spheroidal morphology. These observations are in agreement with previous results demonstrating the dependence of spheroid morphology on RGD ligand density [24] and support the data demonstrating the effect of migration on lineage specification (Fig. 5).

4. Discussion

A key finding in this study is the ability of an engineered biomaterial to continue differentiating stem cells after the removal of exogenous soluble cues both *in vitro* and *in vivo*. We chose the 1-week preconditioning period in this study because it is too short for full differentiation. Indeed, the levels of differentiation markers were low immediately after the preconditioning period, making the contribution of the biomaterial after the 2-week expansion phase readily apparent. While the purpose of this study was to design a clinically applicable biomaterial platform, the system could be used in more mechanistic studies to interrogate the time course and extent of differentiation. For example, in previous studies exploring the relative contributions of soluble factors *versus* substrate mechanics [37], MSCs on soft substrates favoring neurogenesis could still be driven toward osteogenesis or myogenesis if the neurogenic induction period was suitably brief. In our

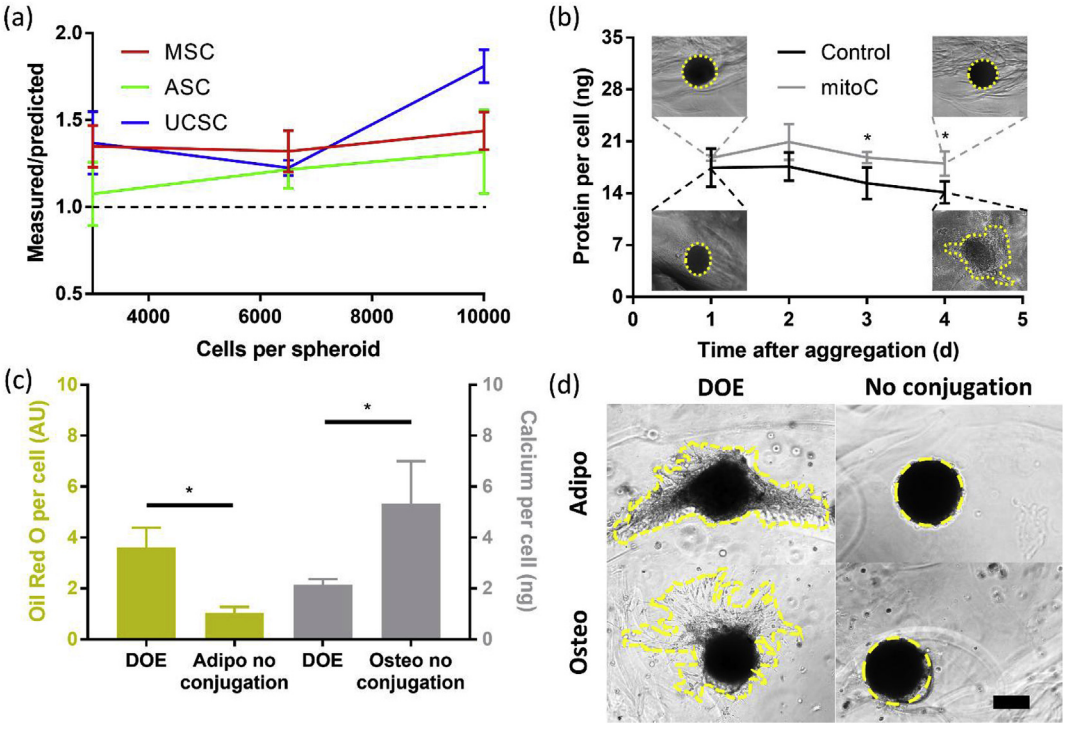

Fig. 5. Migration may account for the multifactorial effect. (**a**) Measured spheroid diameter is larger than that predicted by geometrical models and the difference increases with increasing number of cells, indicating packing density decreases with increasing spheroid cellularity and thus more ECM per cell is available in larger spheroids. (**b**) This effect was simulated in 10,000-cell spheroids by treatment with mitomycin C, which inhibits proliferation and leaves ECM production intact. This resulted in an increase in ECM per cell compared to untreated spheroids, correlating to decreased migration. (**c**) Inhibiting migration by including unconjugated RGD within alginate gels decreased adipogenesis and increased osteogenesis compared to the DOE prediction. In all brightfield images (**d**), yellow dashed lines indicate border of spheroids. Scalebar: 100 μm. (For interpretation of the references to color in this figure legend, the reader is referred to the Web version of this article.)

system, lineage specification by soluble signals occurred on a similar timescale and allows for elucidation of the effects of multiple parameters, either synergistic or antagonistic.

Varying the number of cells per spheroid modulated the extent to which cells could interact with each other, their endogenous matrix, and the alginate hydrogel. Cell migration was greatest in the smallest spheroids, at which point the alginate stiffness and RGD content could exert the greatest effect. All three parameters influence the extent of cell-cell, cell-ECM, and cell-alginate interactions both independently and concomitantly. While we focused on migration in our mechanistic investigation, the combination of spheroid size and alginate formulation will also result in other changes that may affect phenotype retention. For instance, the stiffness sensed by cells within a spheroid is likely different from that in the alginate hydrogel. Both early adipogenesis and osteogenesis involve upregulated collagen I production [23,38,39]. As collagen I fibers possess moduli in the range of 500 MPa [40], the cells may sense a drop in mechanical properties as they migrate into the 15 kPa alginate, further explaining the pro-adipogenic, anti-osteogenic feature of the 100% HM, DS 8, and 3,000 cells/spheroid formulation. In addition, as cells migrate between the differing microenvironments, they may also change which integrins they use to bind. A third possibility is the effect of oxygen gradients within the spheroid. While our previous work demonstrates these gradients are insufficient to result in a hypoxic core at the sizes studied here [32], oxygen tension would still vary depending on spheroid packing density, itself a function of the extent of cells migrating out of the spheroid. A more detailed mechanistic investigation of the mechanobiology between spheroids and our hydrogels will be an interesting subject for future study.

We chose alginate stiffness, RGD content, and spheroid cellularity as our three input parameters, as these are well-studied for their role on cell phenotype. Any number of other parameters, however, could benefit from the employed DOE analysis. For instance, while we characterized the mechanical properties of alginate *via* storage modulus, recent reports have focused on the viscoelastic properties (*e.g.* stress relaxation) of ionically crosslinked alginate [41], providing a potential alternative mechanical input parameter. Biomaterial degradation rate is another possible input that affects *in vivo* vascular invasion and tissue formation. We detected widely varying amounts of residual alginate after the 4-week *in vivo* implantation among the groups (Fig. 6), confirming the various alginate formulations exhibit differences in degradation that may enable cell proliferation and migration.

We envision this system as widely applicable to banked cells, as they could be preconditioned after thaw and combined with previously assembled biomaterial formulations. This prompted the selection of UCSCs in our *in vivo* model, as this cell type is most suited for banking. While the brief preconditioning period is still a requirement for this approach, it represents an advance in translatability over procedures requiring upwards of 4 weeks under *in vitro* culture. The alginate platform is amenable to additional modifications, such as for growth factor delivery, that may further reduce this requirement. In particular, we demonstrated that the various lineages and the different cell types require specific formulations, meaning a highly tunable material is necessary for wide applicability.

These findings demonstrate the ability to engineer biomaterial and spheroid properties tailored to maintain preconditioned phenotype with both lineage and cell type specificity. This study adds to the growing appreciation for the difference between commonly studied progenitor populations for regenerative medicine by elucidating necessary combinations of parameters to drive lineage specification. Notably, the components – alginate and adhesive peptide – are common throughout the approach, underscoring the ability to harness the high tunability of alginate for instructing resident cells. The biomaterial-

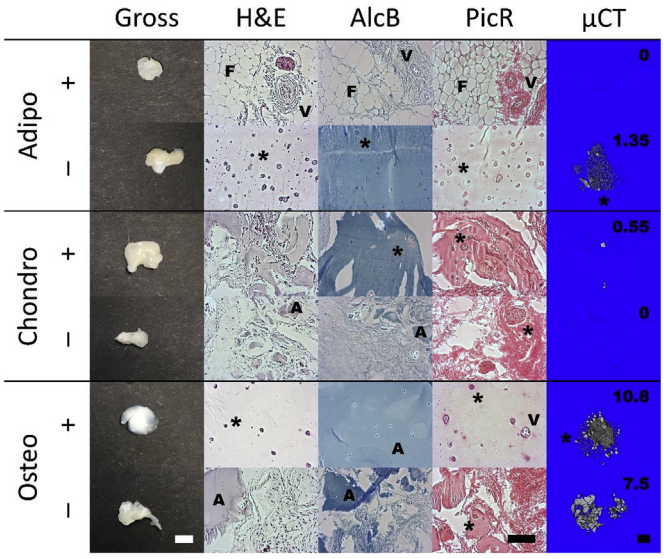

Fig. 6. Phenotype retention is observed *in vivo*. After 4 weeks in a murine subcutaneous site, constructs displayed varying extent of differentiation. Only the maximal adipogenic formulation showed a preponderance of fat ghosts. Purple staining under aldehyde fuchsin for GAG was most apparent in the maximal chondrogenic formulation. Mineralized spheroids were detected in micro-CT in the maximal osteogenic formulation, whereas a shell of mineral was detected in the minimal osteogenic formulation. Numbers indicate hydroxyapatite per volume in mg/cm^3. Red collagen staining under Picrosirius Red localized to spheroids in the maximal osteogenic formulation. The minimal adipogenic formulation also showed positive GAG staining and mineralized spheroids with collagen, but no fat ghosts. F: fat ghosts, V: vessel, *: spheroid, A: alginate. Scalebars: 3 mm (gross images), 200 μm (histological images), 1 mm (micro-CT reconstructions). (For interpretation of the references to color in this figure legend, the reader is referred to the Web version of this article.)

focused approach also facilitates an off-the-shelf product ready to encapsulate isolated or stored cells for rapid assembly of tissue engineered constructs for implantation. Finally, this study demonstrates the capability and importance of the DOE approach in investigating multifactorial systems. The study not only establishes the significant effects of biomaterial stiffness, RGD content, and spheroid cellularity on phenotype retention but also deepens our understanding of the significant interactions between the parameters.

Data availability

The processed data required to reproduce these findings are available to download from Dash at https://doi.org/10.25338/B8RK52.

Author contributions

BPH: conception and design of experiments, data collection and assembly, data analysis and interpretation, manuscript composition.

JNH, AMS, TGF, DES, MLW: data collection and assembly, manuscript composition.

JKL: conception and design of experiments, data analysis and interpretation, manuscript composition, administrative support.

Acknowledgments

Research reported in this publication was supported by the National Institute of Dental and Craniofacial Research of the National Institutes of Health under award number R01 DE025475. The content is solely the responsibility of the authors and does not necessarily represent the official views of the National Institutes of Health. The authors thank Adrienne Wright for her work in isolation and characterization of the UCSCs and Tanya Garcia-Nolen for her assistance in performing the micro-CT scans.

Appendix A. Supplementary data

Supplementary data to this article can be found online at https://doi.org/10.1016/j.biomaterials.2018.10.024.

References

[1] M.F. Pittenger, A.M. Mackay, S.C. Beck, R.K. Jaiswal, R. Douglas, J.D. Mosca, M.A. Moorman, D.W. Simonetti, S. Craig, D.R. Marshak, Multilineage potential of adult human mesenchymal stem cells, Science 284 (5411) (1999) 143–147.
[2] J. Galipeau, L. Sensébé, Mesenchymal stromal cells: clinical challenges and therapeutic opportunities, Cell Stem Cell 22 (6) (2018) 824–833.
[3] J.M. Gimble, A.J. Katz, B.A. Bunnell, Adipose-derived stem cells for regenerative medicine, Circ. Res. 100 (9) (2007) 1249–1260.
[4] K.E. Mitchell, M.L. Weiss, B.M. Mitchell, P. Martin, D. Davis, L. Morales, B. Helwig, M. Beerenstrauch, K. Abou-Easa, T. Hildreth, D. Troyer, S. Medicetty, Matrix cells from Wharton's jelly form neurons and glia, Stem Cell. 21 (1) (2003) 50–60.
[5] D.L. Troyer, M.L. Weiss, Wharton's jelly-derived cells are a primitive stromal cell population, Stem Cell. 26 (3) (2008) 591–599.
[6] A.C. Boquest, A. Noer, P. Collas, Epigenetic programming of mesenchymal stem cells from human adipose tissue, Stem Cell Rev. 2 (4) (2006) 319–329.
[7] E.J. Arnsdorf, P. Tummala, A.B. Castillo, F. Zhang, C.R. Jacobs, The epigenetic mechanism of mechanically induced osteogenic differentiation, J. Biomech. 43 (15) (2010) 2881–2886.
[8] B.P. Hung, D.L. Hutton, K.L. Kozielski, C.J. Bishop, B.A. Naved, J.J. Green, A.I. Caplan, J.M. Gimble, A.H. Dorafshar, W.L. Grayson, Platelet-derived growth factor BB enhances osteogenesis of adipose-derived but not bone marrow-derived mesenchymal stromal/stem cells, Stem Cell. 33 (9) (2015) 2773–2784.
[9] S. Kern, H. Eichler, J. Stoeve, H. Kluter, K. Bieback, Comparative analysis of mesenchymal stem cells from bone marrow, umbilical cord blood, or adipose tissue, Stem Cell. 24 (5) (2006) 1294–1301.
[10] E. Hill, T. Boontheekul, D.J. Mooney, Regulating activation of transplanted cells controls tissue regeneration, Proc. Natl. Acad. Sci. U. S. A. 103 (8) (2006) 2494–2499.
[11] E. Potier, E. Ferreira, A. Meunier, L. Sedel, D. Logeart-Avramoglou, H. Petite, Prolonged hypoxia concomitant with serum deprivation induces massive human mesenchymal stem cell death, Tissue Eng. 13 (6) (2007) 1325–1331.
[12] A.W. James, G. LaChaud, J. Shen, G. Asatrian, V. Nguyen, X. Zhang, K. Ting, C. Soo, A review of the clinical side effects of Bone Morphogenetic Protein-2, Tissue Eng. B Rev. 22 (4) (2016) 284–297.
[13] E.K. Salter, B.C. Goh, B.P. Hung, D.L. Hutton, N.V. Ghone, W.L. Grayson, Bone tissue engineering bioreactors: a role in the clinic? Tissue Eng. B Rev. 18 (1) (2012) 62–75.
[14] I. Martin, T. Smith, D. Wendt, Bioreactor-based roadmap for the translation of tissue engineering strategies into clinical products, Trends Biotechnol. 27 (9) (2009) 495–502.
[15] K.C. Murphy, A.I. Hoch, J.N. Harvestine, D. Zhou, J.K. Leach, Mesenchymal stem cell spheroids retain osteogenic phenotype through alpha2beta1 signaling, Stem Cells Transl. Med. 5 (9) (2016) 1229–1237.
[16] S.S. Ho, K.C. Murphy, B.Y. Binder, C.B. Vissers, J.K. Leach, Increased survival and function of mesenchymal stem cell spheroids entrapped in instructive alginate hydrogels, Stem Cells Transl. Med. 5 (6) (2016) 773–781.
[17] K.Y. Lee, D.J. Mooney, Alginate: properties and biomedical applications, Prog. Polym. Sci. 37 (1) (2012) 106–126.
[18] B.T. Estes, B.O. Diekman, J.M. Gimble, F. Guilak, Isolation of adipose-derived stem cells and their induction to a chondrogenic phenotype, Nat. Protoc. 5 (7) (2010) 1294–1311.
[19] J.R. Smith, A. Cromer, M.L. Weiss, Human umbilical cord mesenchymal stromal cell isolation, expansion, cryopreservation, and characterization, Curr. Prot. Stem Cell Biol. 41 (2017) 1F.18.1–1F.18.23.
[20] B.P. Hung, E.K. Salter, J.P. Temple, G.S. Mundinger, E.N. Brown, P. Brazio, E.D. Rodriguez, W.L. Grayson, Engineering bone grafts with enhanced bone marrow and native scaffolds, Cells Tissues Organs 198 (2) (2013) 87–98.
[21] B.P. Hung, B.A. Naved, E.L. Nyberg, M. Dias, C.A. Holmes, J.H. Elisseeff, A.H. Dorafshar, W.L. Grayson, Three-Dimensional printing of bone extracellular matrix for craniofacial regeneration, ACS Biomater. Sci. Eng. 2 (10) (2016) 1806–1816.
[22] S.Y. Tzeng, B.P. Hung, W.L. Grayson, J.J. Green, Cystamine-terminated poly(beta-amino ester)s for siRNA delivery to human mesenchymal stem cells and enhancement of osteogenic differentiation, Biomaterials 33 (32) (2012) 8142–8151.
[23] F. Langenbach, J. Handschel, Effects of dexamethasone, ascorbic acid and beta-glycerophosphate on the osteogenic differentiation of stem cells in vitro, Stem Cell Res. Ther. 4 (5) (2013) 117.
[24] S.S. Ho, A.T. Keown, B. Addison, J.K. Leach, Cell migration and bone formation from mesenchymal stem cell spheroids in alginate hydrogels are regulated by adhesive ligand density, Biomacromolecules 18 (12) (2017) 4331–4340.
[25] S.S. Ho, B.P. Hung, N. Heyrani, M.A. Lee, J.K. Leach, Hypoxic preconditioning of mesenchymal stem cells with subsequent spheroid formation accelerates repair of segmental bone defects, Stem Cell. 36 (9) (2018) 1393–1403.
[26] O. Jeon, D.S. Alt, S.W. Linderman, E. Alsberg, Biochemical and physical signal

gradients in hydrogels to control stem cell behavior, Adv. Mater. 25 (44) (2013) 6366–6372.
[27] N.A. Kraus, F. Ehebauer, B. Zapp, B. Rudolphi, B.J. Kraus, D. Kraus, Quantitative assessment of adipocyte differentiation in cell culture, Adipocyte 5 (4) (2016) 351–358.
[28] T. Gonzalez-Fernandez, B.N. Sathy, C. Hobbs, G.M. Cunniffe, H.O. McCarthy, N.J. Dunne, V. Nicolosi, F.J. O'Brien, D.J. Kelly, Mesenchymal stem cell fate following non-viral gene transfection strongly depends on the choice of delivery vector, Acta Biomater. 55 (2017) 226–238.
[29] B.O. Enobakhare, D.L. Bader, D.A. Lee, Quantification of sulfated glycosaminoglycans in chondrocyte/alginate cultures, by use of 1,9-dimethylmethylene blue, Anal. Biochem. 243 (1) (1996) 189–191.
[30] G.M. Cunniffe, T. Gonzalez-Fernandez, A. Daly, B.N. Sathy, O. Jeon, E. Alsberg, D.J. Kelly, Three-Dimensional bioprinting of polycaprolactone reinforced gene activated bioinks for bone tissue engineering, Tissue Eng. A 23 (17–18) (2017) 891–900.
[31] T. Gonzalez-Fernandez, E.G. Tierney, G.M. Cunniffe, F.J. O'Brien, D.J. Kelly, Gene delivery of TGF-beta3 and BMP2 in an MSC-laden alginate hydrogel for articular cartilage and endochondral bone tissue engineering, Tissue Eng. A 22 (9–10) (2016) 776–787.
[32] K.C. Murphy, B. Hung, S. Browne-Bourne, D.J. Zhou, J. Yeung, D.C. Genetos, J.K. Leach, Measurement of oxygen tension within mesenchymal stem cell spheroids, J. R. Soc. Interface 14 (127) (2017) 20168051.
[33] B.K. Hall, T. Miyake, All for one and one for all: condensations and the initiation of skeletal development, Bioessays 22 (2) (2000) 138–147.
[34] J.M. Charest, J.P. Califano, S.P. Carey, C.A. Reinhart-King, Fabrication of substrates with defined mechanical properties and topographical features for the study of cell migration, Macromol. Biosci. 12 (1) (2012) 12–20.
[35] S. Dupont, L. Morsut, M. Aragona, E. Enzo, S. Giulitti, M. Cordenonsi, F. Zanconato, J. Le Digabel, M. Forcato, S. Bicciato, N. Elvassore, S. Piccolo, Role of YAP/TAZ in mechanotransduction, Nature 474 (7350) (2011) 179–183.
[36] D.L. Crandall, D.E. Busler, B. McHendry-Rinde, T.M. Groeling, J.G. Kral, Autocrine regulation of human preadipocyte migration by plasminogen activator inhibitor-1, J. Clin. Endocrinol. Metab. 85 (7) (2000) 2609–2614.
[37] A.J. Engler, S. Sen, H.L. Sweeney, D.E. Discher, Matrix elasticity directs stem cell lineage specification, Cell 126 (4) (2006) 677–689.
[38] I. Nakajima, S. Muroya, R. Tanabe, K. Chikuni, Extracellular matrix development during differentiation into adipocytes with a unique increase in type V and VI collagen, Biol. Cell. 94 (3) (2002) 197–203.
[39] Y.Q. Chen, Y.S. Liu, Y.A. Liu, Y.C. Wu, J.C. Del Alamo, A. Chiou, O.K. Lee, Biochemical and physical characterizations of mesenchymal stromal cells along the time course of directed differentiation, Sci. Rep. 6 (2016) 31547.
[40] Y.P. Kato, D.L. Christiansen, R.A. Hahn, S.J. Shieh, J.D. Goldstein, F.H. Silver, Mechanical properties of collagen fibres: a comparison of reconstituted and rat tail tendon fibres, Biomaterials 10 (1) (1989) 38–42.
[41] O. Chaudhuri, L. Gu, D. Klumpers, M. Darnell, S.A. Bencherif, J.C. Weaver, N. Huebsch, H.P. Lee, E. Lippens, G.N. Duda, D.J. Mooney, Hydrogels with tunable stress relaxation regulate stem cell fate and activity, Nat. Mater. 15 (3) (2016) 326–334.